SAND2022-12646J

Graph Theory and Nighttime Imagery based Microgrid Design

Melvin Lugo-Alvarez, Jan Kleissl, Adil Khurram, Matthew Lave, & C. Birk Jones

Abstract— **Reducing the duration and frequency of blackouts in remote communities poses an engineering challenge for grid operators. Outage effects can also be mitigated locally through microgrids. This paper develops a systematic procedure to account for these challenges by creating microgrids prioritizing high value assets within vulnerable communities. Nighttime satellite imagery is used to identify vulnerable communities. Using an asset classification and rating system, multi-asset clusters within these communities are prioritized. Infrastructure data, geographic information systems, satellite imagery, and spectral clustering are used to form and rank microgrid candidates. A microgrid design algorithm is included to guide through the microgrid design process. An application of the methodology is presented using real event, location, and asset data.**

***Index Terms*—**

NOMENCLATURE

$AR(i)$	Total rating of the ith asset
$AT(i)$	Type rating of the ith asset
$SS(i)$	System load size rating of the ith asset
$ACC(i)$	Accessibility rating of the ith asset
$PVP(i)$	Photovoltaic potential rating of the ith asset
S	Unadjusted score for asset rating on a category
α_2	Coefficient of quadratic term of quadratic scale
α_1	Coefficient of linear term of quadratic scale
α_0	Coefficient of constant term of quadratic scale
A	Adjacency matrix of circuit graph
A_{ij}	Number of edges connecting node i to node j
D	Diagonal degree matrix of circuit graph
D_{ii}	Number of edges connected to ith node
L	Laplacian of circuit graph

KEY TERMS AND DEFINITIONS

Asset	Facility or equipment of interest to be powered during a blackout by the proposed microgrids
Cluster	Collection of assets
GIS	Geographic information system
GHI	Global horizontal irradiance: total solar radiation incident on a horizontal surface
KML	Keyhole Markup Language: file format used to display geographic data
Load	Power rating of an asset or cluster
PV	Photovoltaic
Score	Value from 0 to 5 assigned on each of the four categories of the rating system

M. Lugo-Alvarez is a student in the Department of Mechanical and Aerospace Engineering at the University of California San Diego, San Diego, CA, USA
J. Kleissl is with the Center for Energy Research at the University of California San Diego, San Diego, CA, USA
A. Khurram is with the Department of Mechanical and Aerospace Engineering at the University of California San Diego, San Diego, CA, USA
M. Lave is with Sandia National Laboratories, Livermore, CA, USA,
C. B. Jones is with Sandia National Laboratories, Albuquerque, NM, USA

I. INTRODUCTION

Powering remote communities requires overcoming universal challenges such as long line lengths with high power infrastructure installation costs. Recovery from natural disasters is often delayed in remote communities due to access issues and the prioritization of urban centers. A utility typically identifies these isolated customers and prioritizes reconnection by considering cost and labor required, required time, availability of supplies, etc. Due to the remoteness of these locations, reconnection may be a lengthy process. The rearranging of the distribution system infrastructure into a permanent microgrid that allows remote communities to power themselves could reduce outage durations and frequencies.

Geographical information system (GIS) and satellite imagery have been applied to power system restoration after a destructive weather event. For example, [1] shows how to identify destroyed infrastructure using image processing edge finding techniques on daytime satellite imagery. However, power outages in undamaged areas cannot be identified with the technique presented in [1] as light from powered sources cannot be detected using daytime imagery. Previous work with visible nighttime satellite imagery tracked the grid recovery after a major blackout [2]. Historically, power system restoration after a blackout has been handled from the transmission side but distribution level microgrids containing distributed energy resources (DER) are becoming viable alternatives [3][4]. Microgrids present a potential mitigation measure against blackouts and grid instability by combining renewable DERs with storage [5], but it should not be overlooked that higher penetrations of renewable DER may cause grid instability [6]

We combine the work in [2] with population and infrastructure GIS data to provide researchers and distribution grid planners with a methodology to prioritize the selection of permanent microgrids in communities with known vulnerabilities. Vulnerabilities such as being located far from generation sources and experiencing previous blackout events. These microgrids are designed to island in future blackout events. Typical microgrid design algorithms are based around power balancing [7], operational cost optimization [8][9], and line power transmission limits [10]. Identifying affected communities and evaluating the relative importance of a load to the surrounding community is an afterthought. This work aims

to expand the research of microgrid selection and design based around the humanitarian needs of vulnerable communities.

The methodology presented in this paper is an extension of [11] which illustrated how to use nighttime satellite imagery to find blackout areas after a natural disaster, identify the most populated blackout areas, and rate asset clusters as microgrids within the blackout areas on six categories. The six categories of the rating system proposed in [11] are: asset type, system load size, accessibility, cost to power, cluster size, and asset distance to distribution circuit. Three major additions to the work in [11] are presented herein. 1. Category modification to include parameters that can be easily measured or estimated from the circuit and asset topology. The last three categories of the rating system in [11] are discarded and are replaced by the photovoltaic potential category. 2. A modification of the rating and scoring system proposed in [11] to provide better differentiation between scores within a category. 3. The application of spectral clustering which removes the designer bias when producing cluster options and which does not require a predetermined number of clusters or cluster size.

The technique outlined in this work is applicable wherever sufficient data are available regarding nighttime satellite imagery, population data, and distribution system infrastructure. However, we present the real example of the challenging electric power recovery efforts after hurricane María hit Puerto Rico on September 20, 2017[12][13]. In the aftermath some areas were cut off from the power grid for months. The town center may have had power but customers in the surrounding regions were left in the dark.

The paper is organized as follows. Section II describes the proposed methodology that is applied to a test case based on the real assets and feeders in the town of Jayuya, Puerto Rico in Section III. Finally, conclusions are provided in Section IV.

II. Methodology Workflow

The proposed methodology consists of five parts. The blackout area identification and population impact section focuses on identifying the location and number of people affected by a blackout. The asset identification and asset rating sections focus on identifying, classifying, and rating assets in a blackout area. The cluster selection and microgrid design sections focus on creating microgrid candidates out of the selected assets. The key points and flow of the methodology are shown in Fig 1.

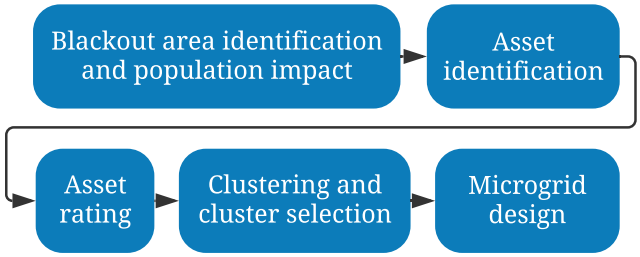

Fig 1 Microgrid identification and design methodology workflow

A. Blackout area identification and customer estimation

The objective in resiliency improvement is to focus on areas where blackouts occur for several days that can be identified by using nighttime satellite imagery. Using satellite imagery to track power recovery was demonstrated in [2]. Nighttime satellite visible imagery as in NASA's black marble product provides composite images, that are processed to remove all light sources that are not man made, such as fires, reflections on clouds, reflections of the moon, etc. [14]. These images are suitable to identify blackout area locations as described next.

To obtain the blackout area locations a mask is created using a pre-blackout baseline and an image during a blackout. An example of the resulting mask after hurricane Maria is shown in Fig 2. Blackouts usually only last from minutes to hours. Therefore, the blackout mask from 2 months after the hurricane suggests a major blackout, motivating the need for microgrid deployments.

Estimating the number of affected customers requires that the mask be geotagged and overlaid onto a population density map (Fig 3). Population data is accessed from the US Census Bureau [15]. The highest granularity at the county subdivision level is used. Puerto Rico has 906 such divisions. The number of affected customers is estimated by multiplying the population density by the blackout area polygon. Priority for microgrid locations is given to polygons with a larger number of affected customers to maximize the number of people benefitting from the location of the resulting microgrid. Fig 4

Fig 4 Top 10% most populated blackout areas 6 months after the hurricane (red). The location of the test case, Jayuya, is circled in blue.[11]

shows the top 10% most populated blackout areas 6 months after the hurricane.

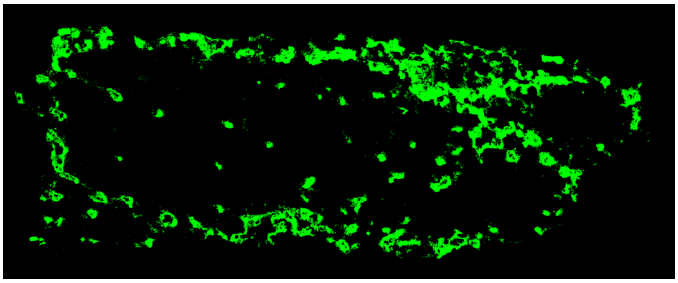

Fig 2 Map of the mask of blackout areas 2 months after hurricane Maria on September 20, 2017. Blackout areas are marked in green[11]. For a scale see Fig. 3.

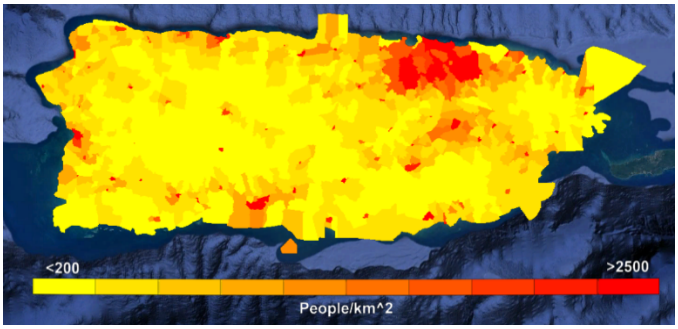

Fig 3 Population density color map, where red is higher yellow is lower. The map was derived from the population and land area data found in [15].

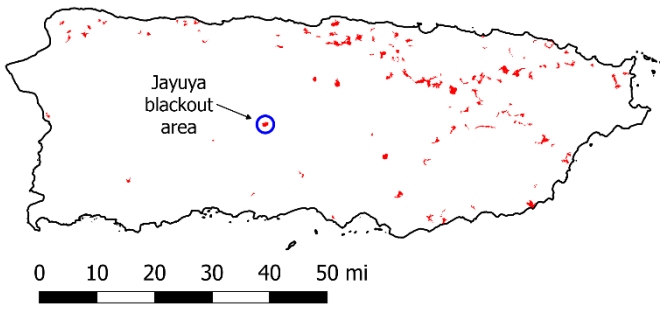

Fig 4 Top 10% most populated blackout areas 6 months after the hurricane (red). The location of the test case, Jayuya, is circled in blue.[11]

B. Asset identification

After the blackout areas have been identified, the coordinates of assets within these locations are obtained from KML files as explained in this subsection.

The coordinates of radio, water, telecom, and emergency shelter assets were obtained from [16] as KML files. Google Earth [17] and Google Maps [18] searches yielded KML files of critical assets such as supermarkets, restaurants, healthcare facilities, fueling stations, police stations, and firefighting stations as well as non-critical assets such as government offices, schools, courthouses, postal offices, places of worship, and private businesses. From the KML files the coordinates, physical addresses, and types for each asset were extracted. The KML files were imported into Google Earth for visualization.

Assets are then individually rated as described in section II.C. The asset ratings of all assets in a cluster are combined and the clusters are ranked and selected according to the procedure described in section II.D.

C. Asset rating

Prior to clustering, all assets are assigned a rating according to 4 categories: asset type, system size, accessibility, and photovoltaic potential. The categories defined in Table 1 were selected as an indirect way to quantify the cost and benefit of including a particular asset in the microgrid and are described further below.

Asset type: The asset search is performed using the keywords listed in the asset type category of **Error! Reference source not found.**. Therefore, asset type is readily detected during the asset identification stage and the score assigned by matching key and value pairs through scripting. Higher values are assigned to services and infrastructure that have a broader geographical impact on many people. Lower values are assigned for local impact on a few people. Critical assets are those rated 3 – 5 in the first (Asset type) column of Table 1. Other assets, rated 0 – 2, are not critical, but are still included. That is because if assets rated 0-2 are near critical assets it may still be beneficial to include in a cluster. Critical assets may benefit from the inclusion of non-critical assets under certain conditions, e.g., when the non-critical asset has large PV potential or good accessibility.

System load size: The system load for an asset, when not obtained directly from the asset administrator or the local utility, can be estimated using the TMY2 reference buildings of [19]. The system load size score assignment is automated through scripting using the power limits listed in **Error! Reference source not found.**. The microgrid design assumption is that each asset can provide sufficient power for itself. Smaller loads are scored higher as these are less costly to power.

Accessibility: Evaluating accessibility requires visual inspection of satellite imagery and road maps of the blackout area. Assets located in accessible places are favored over those located in remote regions. Accessibility is an important parameter to consider as easy access to service providing assets improves the surrounding community resilience. A microgrid consisting of accessible assets has lower construction and maintenance costs compared to a microgrid with inaccessible assets. Asset access characteristics to consider when evaluating accessibility include number of access points, status of access points (e.g., paved, unpaved, overgrown, well maintained, etc.), means of transportation required to access asset (e.g., unmodified street vehicle, off-road capable vehicles, all-terrain vehicles, amphibious vehicles, aircraft, etc.). The accessibility column of **Error! Reference source not found.** shows the 0 to 5 scoring of the access characteristics.

Photovoltaic Potential: Solar photovoltaic (PV) power is the selected renewable generation source for the assets in this work. Estimated peak PV power potential for an asset is calculated by measuring the available roof top area and multiplying roof top area by the peak global horizontal irradiance (GHI) [20] of the asset's location. Roof top area is determined using Google Earth, QGIS [21], and OpenStreetMap [22] tools. The photovoltaic potential is defined as the PV potential divided by the system peak load as shown in (1) and assigned a score as described by **Error! Reference source not found.**. The maximum score of 5 is assigned to assets with a PV potential greater or equal to 135%. The 135% cutoff point is based on the PV system sizing in [23], where a PV system size 1.35 times the load size was enough to offset the yearly energy requirements of an asset in Albuquerque, NM. The 1.35 factor is similar to the recommendations in [24] for PV system to load sizing, where a factor of 1.3 – 1.4 is recommended for critical loads or locations with low irradiance.

$$\text{PV potential \%} = \frac{\text{Peak PV potential (kW)}}{\text{System load size (kW)}} \times 100\% \quad (1)$$

Combined Rating: Each asset is assigned a score on the four categories: asset type (AT), system size (SS), accessibility (ACC), and photovoltaic potential (PVP) criteria. Each score is converted from a linear 0-5 score to a quadratic 0-100 score. Conversion from linear to quadratic scaling increases the relative importance of high scores. Quadratic scaling prevents a cluster of many low rated assets from scoring better than a cluster with a few high rated assets. The relative importance of each score within the rating scale is tuned by adjusting the coefficients α_2, α_1, α_0 of (2). The coefficients are selected such that the highest score 5, has a maximum rating of 100 as shown

in Fig 5. The score (S) from 0 to 5 for each category as obtained from **Error! Reference source not found.** is converted from a linear to quadratic scale, per the example for *AT(i)*

$$AT(i) = \alpha_2 S^2 + \alpha_1 S + \alpha_0 \qquad (2)$$

The total asset rating (AR) of the i-th asset is the sum of each of the categories as follow,

$$AR(i) = AT(i) + SS(i) + ACC(i) + PVP(i) \quad (3)$$

The current rating system assigns the same coefficients α_2, α_1, α_0 to all four categories. It is possible to assign different coefficients to each category and tune the characteristics of the winning set of clusters.

Table 1 Decision matrix for asset scoring

Score	Asset type	System load size	Accessibility	Photovoltaic Potential
5	Radio, water, telecom, shelters, supermarkets, restaurants, fuel	< 10kW	More than one paved access point in good condition requiring no special vehicles for access	>=135% of load
4	Healthcare Facilities	< 50kW	Single paved access point in good condition (e.g., dead-end road, cul-de-sac) requiring no special vehicles for access	<135% of load
3	Police stations, firefighting stations, other emergency personnel	< 100kW	Well maintained unpaved access point(s), requiring an off-road capable vehicle for access	<100% of load
2	Govt. offices, courthouses, schools, postal offices, public buildings	< 500kW	Paved or unpaved access point(s) are in poor condition	<75% of load
1	Places of worship, Private businesses	< 1MW	Access point(s) are susceptible to damage or danger (e.g., areas prone to flooding, landslides, black ice)	<50%
0	Residential Loads	> 1MW	Requires special vehicle for access (all-terrain vehicle, amphibious, aircraft) regardless of access point status	<25% of load

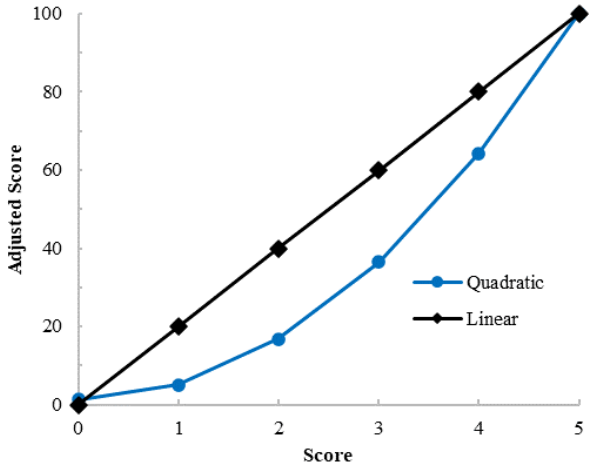

Fig 5 Comparison between linear and quadratic adjusted scores illustrated in this figure. The blue quadratic scale is used in the test case in Section IV with coefficients α_2=4, α_1=-0.25, α_0=1.25.

D. Clustering and cluster selection

Clustering groups the assets into suitable microgrid candidates. Asset groupings are accomplished via spectral clustering with the aid of graph theory and the radial nature of a distribution system feeder. Other potential clustering methods include K-means clustering that uses Euclidean distance to identify clusters. Spectral clustering is preferred over a simple Euclidian distance clustering approach as spectral clustering considers the circuit geometry. Assets will not be grouped together if new circuit lines would have to be built to join them; the clusters will only be created by removing existing circuit lines. For an introduction to spectral clustering with K-means the reader is referred to [25].

The buses and lines of a distribution system can be modeled as a graph G with n nodes. The mostly radial nature of a distribution feeder means that feeders can be modeled as a tree graph. Some important properties of tree graphs are: there are no circles (no closed loop) collections of nodes and edges in a tree, any two nodes are connected by exactly one path, and removing any edge results in a forest which is a collection of trees [26]. Converting a tree into a collection of smaller trees means that all clusters created by disconnecting from the main circuit conserve their radial nature. The feeder is modeled as an undirected graph and is represented by the adjacency matrix A, where A is an n by n matrix and n is the number of buses. The entries of A, a_{ij} are the number of edges between nodes i and j [25]. A is a sparse symmetric matrix. The diagonal degree matrix D and the graph Laplacian L are derived from the adjacency matrix as,

$$D_{ii} = \sum_{j=1}^{n} A_{ij}, \qquad (4)$$

$$L := D - A. \qquad (5)$$

Representing the feeder as a graph and calculating the A, D, and L matrices facilitates cluster creation by means of spectral clustering. The steps for spectral clustering are:

1. Define adjacency matrix A of the feeder.
2. Compute degree matrix D from the adjacency matrix.
3. Compute Laplacian L from degree and adjacency matrices.
4. Find eigenvectors and eigenvalues of the Laplacian.

5. Use K-means to find as many clusters as possible by computing K-means *n-2* times where the desired number of clusters for each iteration is 2, 3, 4, …, *n-1*.

No assumptions are made as to the appropriate number of clusters based on the eigenvalue heuristic or other methods as described in [25] prior to executing the K-means step. Clusters produced by K-means that do not contain all the selected assets and interconnection points in a single continuous graph are discarded. Additionally, the trivial cases of all assets are in a single cluster, all single-asset clusters and clusters with no assets are preemptively discarded.

Clusters are then rated based on the assigned ratings and circuit length. The cluster rating is defined as the sum of the ratings for all assets in a cluster $\sum AR(i)$ divided by the cluster circuit length given by

$$\text{Cluster Rating} = \frac{\sum \text{AR(i)}}{\text{Cluster circuit length}}, \quad (6)$$

where the circuit length is the sum of the length of all the edges in the cluster's graph. Dividing the sum of asset ratings by the circuit length produces a rating per circuit length value for each cluster. The cluster rating as defined in (6) is an asset value density metric that prioritizes more dense clusters that are easier to coordinate and maintain. The ranking and down-selection process to get from all possible clusters to unique and preferred clusters is shown in Fig. 6. The cluster selection algorithm does not guarantee that all assets will be part of a cluster.

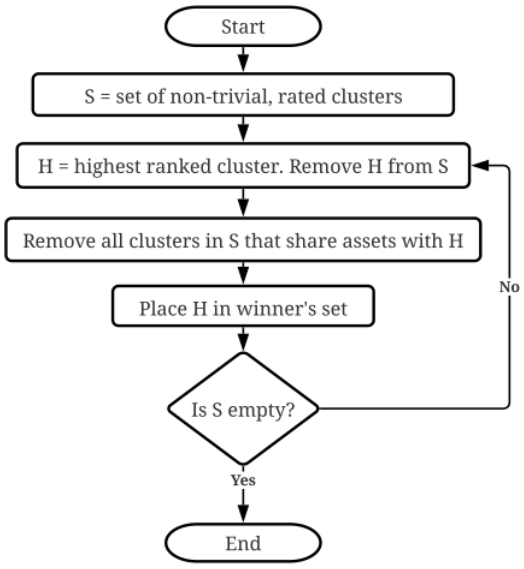

Fig. 6 Cluster ranking and selection algorithm.

E. Microgrid design

After cluster selection, all that is left is to decide how the loads will be powered. The flowchart in Fig 7 illustrates the decision and design process and ensures that all loads within a cluster can be supplied. There are four major decisions that control the path through the flow chart as explained next.

The first decision concerns the selection of a surplus load factor. The surplus load factor allows the designer to oversize the energy supply of the microgrid to allow for future expansion. Large surplus load factors increase the implementation cost whereas small surplus load factors are recommended if little to no load increase is projected over the life of the microgrid. The surplus load factor selection is at the discretion of the person performing the microgrid design. In this paper, unity surplus load factor is considered for illustration purpose.

The second major decision involves the inclusion of renewable DERs. The viability of different types of renewable DER depends on the geographic location of the microgrid. Solar photovoltaic power is the renewable DER selected in this work. The final amount of renewable generation is adjusted until the required capacity is met.

The third major decision involves the inclusion of storage. If a microgrid is designed to be powered solely by renewable solar PV power it must include storage. The storage size depends on the PV generation and nighttime energy consumption. The blackout in the example provided in Section II lasted 6 months which would require a microgrid that can island permanently.

The fourth major decision involves the inclusion of non-renewable generation sources. The energy capacity of non-renewable generation sources in the flowchart is defined as the total system load minus the renewable generation capacity. The amount of fuel storage required is based on the expected off-grid operation time or the expected resupply time after a major event. If the cluster energy consumption cannot be met by PV, non-critical asset load can be curtailed , or the remaining percentage of load can be provided by the non-renewable generation during periods of insufficient PV generation.

III. Test Case

The test case portrays the application of the methodology introduced in Section II for a location in Puerto Rico in three parts. The first part, location, succinctly covers section II.A. The second part, assets and clustering, combines section II.B, section II.C, and section II.D. The last section, PV and microgrid design, covers the PV based microgrid solution for the top-rated cluster in the test location.

A. Location

The test case is a substation located in the town of Jayuya, PR.

Fig 4 Top 10% most populated blackout areas 6 months after the hurricane (red). The location of the test case, Jayuya, is circled in blue.[11]

Fig 4 shows the location of Jayuya within Puerto Rico. Fig 8 shows a close-up of Jayuya, the substation, and the blackout area. The blackout area has an estimated population of 417 and is ranked within the top five percent most populated blackout areas. The Jayuya substation has 5 feeders. Feeder Jayuya-A, selected for the test case, contains most of the critical assets in the town center and additional assets several miles away from the town center. The reduced network representation of the test feeder is shown in Fig 9. The combination of closely grouped assets and remote assets on the same feeder provide a way to showcase spectral clustering and the proposed cluster ranking methodology.

B. Assets and clustering

A total of 41 assets were found around the Jayuya-A feeder after performing a search for the asset types listed in section II.B. An additional 20 interconnection points were selected. Interconnection points do not directly provide microgrid benefits and are therefore assigned a zero score in all categories but are required to connect all assets into a single network. A breakdown of the asset type score for the 41 assets is presented in Table 2. Other scores are omitted here for brevity. The assets were rated as described in section II.C. Since asset loads were not available, they had to be estimated using the TMY2 commercial reference buildings [19].

Table 2 Breakdown of asset type score for the Jayuya-A test case

Asset type score	0	1	2	3	4	5
Count	0	6	4	1	3	27
Percent of total	0%	15%	10%	2%	7%	66%

Performing spectral clustering on the feeder created 184 unique viable cluster options. Of the 184 options, Table 3 shows the 12 clusters that were selected as winners. The top 12 winners are shown in Fig 10. Due to the normalization of the cluster score by the circuit length, the cluster ranking is strongly correlated with the inverse of the circuit length. For example, the three most highly ranked clusters have circuit lengths of less than 120 m. The average size of the winning cluster is 2.83 assets. The winning 12 cluster options cover 34 or 81% of the 41 assets on the feeder (Fig 11).

Table 3 Winning clusters summary

ID	$\sum AR(i)$	Circuit length (m)	$\frac{\sum AR(i)}{Circuit\ length}$	Number of assets	Power rating of cluster (kW)
84	1065.00	107	9.97	3	48
154	617.50	110	5.62	2	95
97	566.25	119	4.77	2	34
37	1572.00	369	4.26	5	126
85	550.25	200	2.75	2	34
27	812.00	529	1.53	3	217
16	796.50	597	1.33	3	45
28	836.00	771	1.08	3	34
26	633.50	641	0.99	2	271
25	946.00	1622	0.58	3	476
135	1191.75	4572	0.26	4	599
33	531.00	2342	0.23	2	30
Average	843.15	998	2.78	2.83	167

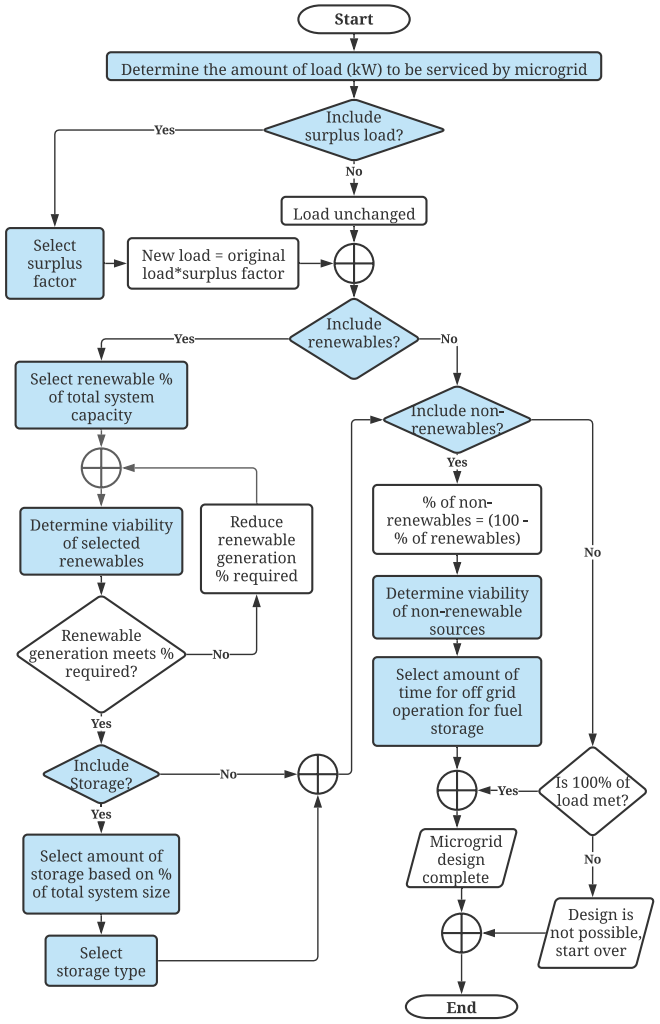

Fig 7 Flow chart for the design of the generation resources for a microgrid. User input is required for the light blue colored boxes. Modified version of flowchart found in [8].

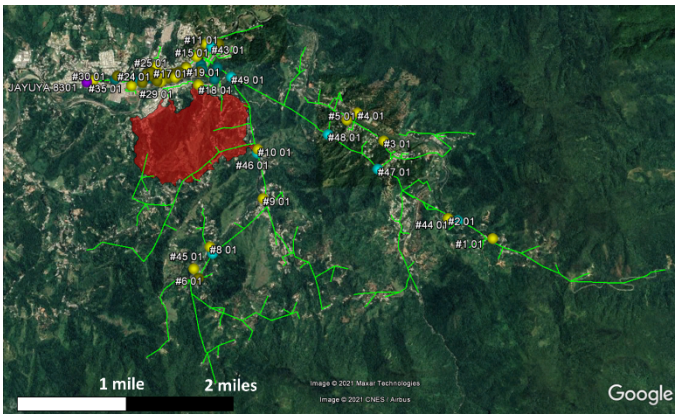

Fig 8 Jayuya-A feeder. Assets are shown in yellow, interconnection points in cyan, and the substation in purple. The blackout area after Hurricane Maria is shown as a red polygon.

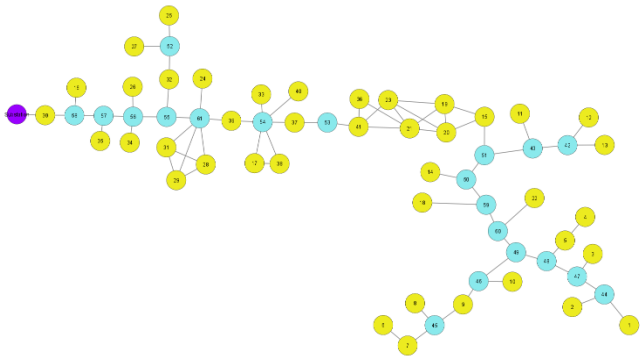

Fig 9 Reduced network model of the Jayuya-A feeder. Assets are shown in yellow, interconnection points in cyan, and the substation in purple.

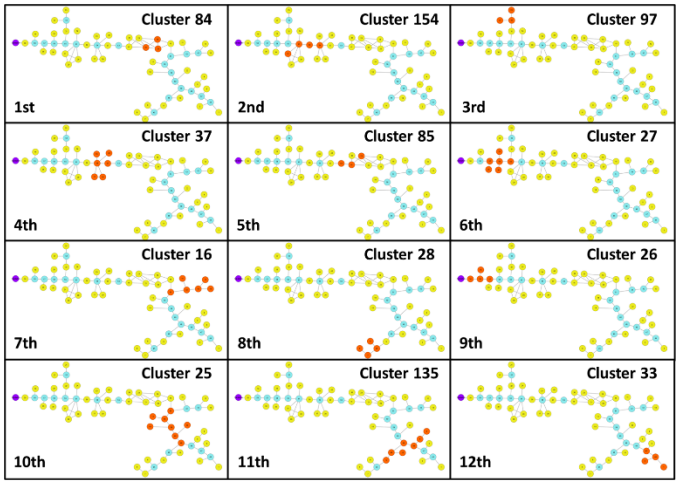

Fig 10 Top 12 winners in ranked clusters. Assets selected as part of the cluster are shown in orange, unselected assets are yellow, interconnection points are blue, and the substation is purple.

Fig 11 Combination of all winning clusters. Unselected assets are shown in yellow. The substation is shown in purple. 81% of the assets and 100% of the interconnection points have been selected.

C. PV and microgrid design

The top ranked cluster, cluster 84 (Fig. 10), was selected for the PV and microgrid design. Cluster 84 consists of three assets: a small outpatient clinic, a pharmacy, and a cafeteria. Cluster 84 has the shortest circuit length of the winners, and all three included assets are scored 4 or better on asset type, system load size, and accessibility categories. The combination of highly scoring assets and short circuit length made cluster 84 the winner. The assets are in the center of Jayuya and are connected by a single feeder segment (see Fig 12). The asset characteristics are summarized in Table 4 and the microgrid characteristics are summarized in Table 5.

Cluster 84 illustrates how assets benefit from pooling resources together. The PV system consists of 182 PV modules of type [27]. The total rooftop area of the assets is 363 m^2, which is greater than the 258 m^2 area required for a PV system to match the peak load of all three assets but not enough for the total energy required by the assets. Therefore, 30% of the microgrid energy will be supplied by non-renewable sources viz a diesel generator. The microgrid contains a 20 kW diesel generator coupled to a 250 US gal. tank which is able to sustain the 14.4 kW load for eight days [28]. The battery energy storage system (BESS) is designed to be 48 kW and 576 kWh. The BESS can store half a day's worth of energy for the microgrid when operated at constant peak load. The BESS sizing assumes coincident peak load and could be refined but is outside the scope of this work.

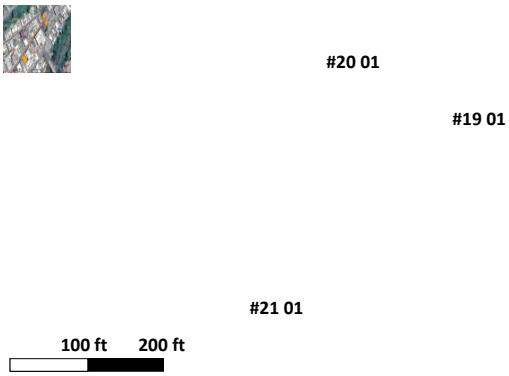

Fig 12 Map of cluster 84 containing assets 19, 20, 21 and no interconnection points. The orange line is the common circuit line. The orange polygons are asset roof areas.

Table 4 Cluster 84 asset characteristics

Asset ID	19	20	21
Asset name	Policlinica Castañer	Farmacia Padua	Cafeteria Rodriguez
Type	Clinic	Pharmacy	Restaurant
Asset roof area (m^2)	83	102	178
System load size (kW)	9	6	33
PV potential (kW)	13	16	29
PV potential %	152	268	86
Load Energy (kWh/day)	84	67	376
Asset type score	4	5	5
System load size score	5	5	4
Accessibility score	5	5	5
PV potential score	5	5	3

Table 5 Microgrid characteristics

Microgrid Sizing Characteristics	
Total cluster load (kW)	48
Total cluster energy (kWh/day)	526
Surplus factor	1
New total load (kW)	48
New total energy (kWh)	526
Percent renewable energy (%)	70
Percent non-renewable energy (%)	30
Peak power supplied by renewables (kW)	48
Peak power supplied by non-renewables (kW)	48
Renewable energy requirement (kWh/day)	368
Non-renewable energy requirement (kWh/day)	158

Solar System Sizing	
GHI for Jayuya (kWh/m^2/day)	5.1
Selected solar module efficiency (%)	20
Total panel area (m^2)	361
Area of selected panel (m^2)	1.98
Number of panels	182
Battery Energy Storage System	
Percent of total system power capacity (%)	100
Storage peak power (kW)	48
Isolated operation duration (days)	0.5
Total operation time (hrs)	12
Total energy required from storage (kWh)	576
Diesel Generator and Fuel Storage	
Generator size (kW)	20
Operational load (kW)	14.4
Fuel consumption at operational load (US gal/hr)	1.3
Diesel tank size (US gal)	250
Duration at operational load (days)	8

IV. Conclusion and Future Work

The methodology presented in this work suggests multi-asset clusters for areas that are frequently affected by blackouts. The clusters are designed with a bottom-up approach where pooling of resources such as PV and utilizing existing power lines over short distances can provide more economical and more resilient clusters. In top-down approaches only obvious critical assets such as hospitals, airport terminals, and supermarkets are typically selected for resilient microgrids resulting in significant capital investments associated with resilient power systems for large single critical assets. In a bottom-up approach critical and non-critical assets in combination with existing circuit topologies are considered with the goal of pooling resources and reducing the number of modifications required on a feeder to implement a microgrid. Using existing power lines requires the use of grid forming inverters [29] and disconnects upstream and downstream of the microgrid. On the other hand, constructing a microgrid with unconstrained circuit topology may involve building new power lines and poles, setting aside land for power line right-of-way [30] or installing underground power lines in addition to the modifications required when building with existing power lines. The proposed method provides a rapid and insightful decision support tool for the pre-feasibility stage of microgrid cluster screening. Preselected clusters would then have to be evaluated with the affected property owners and the utility to establish feasibility, engineering, and cost. The tool is especially useful for screening large areas that are frequently affected to power outages.

The spectral clustering portion of this work is based on an undirected unweighted graph and an unnormalized graph Laplacian. Information of asset characteristics such as circuit length between assets, asset type, load size, and PV potential could be encoded as weights in the graph. Future work direction for this work would involve the weighted graph and the possible reduction in the number of steps in the methodology after spectral clustering.

V. Acknowledgements

Sandia National Laboratories is a multimission laboratory managed and operated by National Technology & Engineering Solutions of Sandia, LLC, a wholly owned subsidiary of Honeywell International Inc., for the U.S. Department of Energy's National Nuclear Security Administration under contract DE-NA0003525. This work was supported by the Department of Energy's Office of Electricity and the Federal Emergency Management Agency (FEMA).

References

[1] Jamshad, R., Qureshi, M. and Grijalva, S., 2018. Geographic Information Systems (GIS) Image Analysis for Prioritizing Power System Restoration. 2018 Clemson University Power Systems Conference (PSC), [online] Available at: <https://ieeexplore.ieee.org/document/8664080> [Accessed 26 October 2021].

[2] M. O. Roman, E. C. Stokes, R. Shrestha, Z. Wang, L. Schultz, E. A. S. Carlo and e. al., "Satellite-based assessment of electricity restoration efforts in Puerto Rico after Hurricane Maria," PLoS ONE, 28 June 2019.

[3] L. Yang, Y. Zhao, C. Wang, P. Gao and J. Hao, "Resilience-Oriented Hierarchical Service Restoration in Distribution System Considering Microgrids", *IEEE Access*, vol. 7, pp. 152729-152743, 2019. Available: 10.1109/access.2019.2948372 [Accessed 11 November 2021].

[4] M. Braun et al., "The Future of Power System Restoration: Using Distributed Energy Resources as a Force to Get Back Online", *IEEE Power and Energy Magazine*, vol. 16, no. 6, pp. 30-41, 2018. Available: 10.1109/mpe.2018.2864227.

[5] Saleh, M.S., Althaibani, A., Esa, Y., Mhandi, Y. and Mohamed, A.A., 2015. Impact of clustering microgrids on their stability and resilience during blackouts. 2015 International Conference on Smart Grid and Clean Energy Technologies (ICSGCE), [online] Available at: <https://ieeexplore.ieee.org/document/7454295> [Accessed 26 October 2021].

[6] Dudurych, I., 2021. The Impact of Renewables on Operational Security: Operating Power Systems That Have Extremely High Penetrations of Nonsynchronous Renewable Sources. IEEE Power and Energy Magazine, [online] 19(2), pp.37-45. Available at: <https://ieeexplore.ieee.org/document/9360581> [Accessed 26 October 2021].

[7] H. Chen and E. Cotilla-Sanchez, "A Power-Balanced Clustering Algorithm to Improve Electrical Infrastructure Resiliency", in *20th Power Systems Computation Conference*, Dublin, Ireland, 2018.

[8] Che, L., Zhang, X., Shahidehpour, M., Alabdulwahab, A. and Abusorrah, A., 2017. Optimal Interconnection Planning of Community Microgrids With Renewable Energy Sources. IEEE Transactions on Smart Grid, [online] 8(3), pp.1054-1063. Available at: <https://ieeexplore.ieee.org/document/7185424> [Accessed 26 October 2021].

[9] Rosenberg, M., Fletcher, J., Reynolds, M., French, T. and While, L., 2019. Identifying Isolated Microgrids in Rural Areas : An Evolutionary Algorithm Approach for a Graph Clustering Problem. 2019 IEEE Congress on Evolutionary Computation (CEC), [online] Available at: <https://ieeexplore.ieee.org/document/8790232> [Accessed 26 October 2021].

[10] Biswas, R., Pal, A., Werho, T. and Vittal, V., 2021. A Graph Theoretic Approach to Power System Vulnerability Identification. IEEE Transactions on Power Systems, [online] 36(2), pp.923-935. Available at: <https://ieeexplore.ieee.org/document/9144487> [Accessed 26 October 2021].

[11] M. Lugo-Alvarez, R. Broderick and E. Ortiz-Rivera, "Strategic Placement and Design of Microgrids using Nighttime Imagery", *2020 47th IEEE Photovoltaic Specialists Conference (PVSC)*, 2020. Available: 10.1109/pvsc45281.2020.9300903 [Accessed 15 January 2021].

[12] Pasch, R., Penny, A. and Berg, R., 2019. *Hurricane Maria (AL152017)*. National Hurricane Center Tropical Cyclone Report. [online] National Oceanic and Atmospheric Administration. Available at: <https://www.nhc.noaa.gov/data/tcr/AL152017_Maria.pdf> [Accessed 11 November 2021].

[13] M. Lugo-Alvarez, "Improving Energy Resource Availability and Resilience with the Strategic Placement of Microgrids", Master's Thesis, University of Puerto Rico at Mayaguez, 2019 https://hdl.handle.net/20.500.11801/2554.

[14] M. O. Román, Z. Wang, Q. Sun, V. Kalb, S. D. Miller and E. al., "NASA's Black Marble nighttime lights product suite," Remote Sensing of Environment, vol. 210, pp. 113-143, 2018.

[15] United States Census Bureau, "Geographies: TIGER/Line with Selected Demographic and Economic Data," 2010. [Online]. Available: https://www.census.gov/geographies/mapping-files/time-series/geo/tiger-data.2010.html.

[16] U. D. o. H. Security, "Homeland Infrastructure Foundation-Level Data (HIFLD) Open Data," 2017. [Online]. Available: https://hifld-geoplatform.opendata.arcgis.com/.

[17] Google, "Google Earth", *Earth.google.com*, 2021. [Online]. Available: https://earth.google.com/. [Accessed: 17- Oct- 2021].

[18] Maps.google.com. 2021. *Google Maps*. [online] Available at: <https://maps.google.com/> [Accessed: 17- Oct- 2021].

[19] Catalog.data.gov. 2021. *Commercial and Residential Hourly Load Profiles for all TMY3 Locations in the United States - CKAN*. [online] Available at: <https://catalog.data.gov/dataset/commercial-and-residential-hourly-load-profiles-for-all-tmy3-locations-in-the-united-state-bbc75> [Accessed 10 September 2021].

[20] NREL, "NSRDB Data Viewer Multi Year PSM Global Horizontal Irradiance," NREL, Denver, Colorado, 2019

[21] "OpenStreetMap", *OpenStreetMap*, 2021. [Online]. Available: https://www.openstreetmap.org/. [Accessed: 17- Oct- 2021].

[22] QGIS Development Team, "Welcome to the QGIS project!", *Qgis.osgeo.org*, 2021. [Online]. Available: http://qgis.osgeo.org. [Accessed: 17- Oct- 2021].

[23] C.B. Jones, M. Lave, M. Reno, R. Darbali-Zamora, A. Summers and S. Hossain-McKenzie, "Volt-Var Curve Reactive Power Control Requirements and Risks for Feeders with Distributed Roof-Top Photovoltaic Systems", *Energies*, vol. 13, no. 17, p. 4303, 2020. Available: 10.3390/en13174303 [Accessed 27 October 2021].

[24] "IEEE Recommended Practice for Sizing Stand-Alone Photovoltaic (PV) Systems," in IEEE Std 1562-2021 (Revision of IEEE Std 1562-2007) , vol., no., pp.1-35, 3 Sept. 2021, doi: 10.1109/IEEESTD.2021.9528316.

[25] von Luxburg, U., 2007. A tutorial on spectral clustering. Statistics and Computing, [online] 17(4), pp.395-416. Available at: <https://link.springer.com/article/10.1007/s11222-007-9033-z> [Accessed 26 April 2020].

[26] R. Wilson, *Introduction to graph theory*, 4th ed. Essex, England: Addison Wesley Longman Publishing Company, 1996.

[27] Peimar Italian Photovoltaic Modules, "SM400M", Peimar, 2020. [online] Available at:<https://sunwatts.com/content/specs/Peimar%20SM400M.pdf> [Accessed 12 November 2021

[28] "Approximate Diesel Generator Fuel Consumption Chart", *Generatorsource.com*, 2021. [Online]. Available: https://www.generatorsource.com/Diesel_Fuel_Consumption.aspx. [Accessed: 23- Nov- 2021].

[29] Lin, Y., 2020. *Grid-Forming Inverters – Enabling the Next Generation Grid*., Available https://www.nrel.gov/aries/assets/pdfs/pegi-lin.pdf. [Accessed: 12- Nov- 2021]

[30] Sdge.com. 2021. *New land services | San Diego Gas & Electric*. [online] Available at: <https://www.sdge.com/landservices> [Accessed 12 November 2021].